Correlation between strain rate and seismicity in different tectonic settings

Yuxuan Chen*[1,2] and Mian Liu[2]

[1] School of Geodesy and Geomatics, Wuhan University, Wuhan 430079, China

[2] Dept. of Geological Sciences, University of Missouri, Columbia, MO 65211, USA.

*Corresponding author: Yuxuan Chen (yc2023@whu.edu.cn)

Address: 129 Luoyu Road, Wuhan 430079, China

Declaration of Competing Interests

The authors acknowledge that there are no conflicts of interest recorded.

Abstract

Geodetic strain rate characterizes present-day crustal deformation and therefore may be used as a spatial predictor for earthquakes. However, the reported correlation between strain rates and seismicity varies significantly in different places. Here, we systematically study the correlation between strain rate, seismicity, and seismic moment in six regions representing typical plate boundary zones, diffuse plate boundary regions, and continental interiors. We quantify the strain rate-seismicity correlation using a method similar to the Molchan error diagram and area skill scores. We find that the correlation between strain rate and seismicity varies with different tectonic settings that can be characterized by the mean strain rates. Strong correlations are found in typical plate boundary zones where strain rates are high and concentrated at major fault zones, whereas poor or no correlations are found in stable continental interiors with low strain rates. The correlation between strain rate and seismicity is also time-dependent: it is stronger in seismically active periods but weaker during periods of relative quiescence. These temporal variations can be useful for hazard assessment.

Introduction

The advancement of space-based geodesy in the past decades has provided great details of present-day crustal deformation. Geodetic strain rates indicate where and how fast strain is accumulating near Earth's surface. Because much of the strain is elastic and will be released by earthquakes, geodetic strain rates may be used as a spatial predictor for earthquakes. On a global scale, Kreemer *et al.* (2002) found that seismicity rates of shallow earthquakes are correlated with strain rates in subduction zones and active continental plate boundaries. In California and Nevada, large earthquakes are concentrated in the San Andreas Fault system, the Eastern

California Shear Zone, and the Walker Lane shear zone, where strain rates are high and well correlated with seismicity (Shen *et al.*, 2007; Zeng *et al.*, 2018; Kreemer and Young, 2022). In the Tibetan Plateau, higher strain rate regions have higher background seismicity rates (Stevens and Avouac, 2021), hence strain rate is used in some probabilistic seismic hazard assessments (Shen *et al.*, 2007; Stevens and Avouac, 2021).

However, poor correlation between strain rate and seismicity has been found in other places. In North China, active tectonic zones have both high strain rates and seismicity rates, but some low strain rate regions have significant modern seismicity and large historical earthquakes (Liu and Wang, 2012; Chen *et al.*, 2021). In stable North America, low strain rates are found in the major seismic zones such as the Charleston, South Carolina area, the Eastern Tennessee Seismic Zone, and the New Madrid Seismic Zone (NMSZ) (Calais *et al.*, 2016; Kreemer *et al.*, 2018). In the Saint Lawrence Valley, eastern Canada, Tarayoun *et al.* (2018) found that high strain rate is concentrated in ancient rift zones where modern seismicity and large historical earthquakes are clustered, but no systematic correlation is found between seismicity and geodetic strain rate in the whole region.

The correlation between strain rate and seismicity could also be time-dependent. In California and Nevada, the $M \geq 4$ background earthquakes gradually changed from a diffuse distribution in the whole region (1933-1980s) to a concentrated distribution in high strain rate areas (1980s-2016), along with increasing $M \geq 6.5$ events (Zeng *et al.*, 2018). In mainland China, temporal variations of the correlation between strain rate and seismicity are also observed (Wu *et al.*, 2021). Comparison of such temporal variations of seismicity with geodetic strain rates could provide useful insights for hazard assessment.

In this study, we systematically analyzed and quantified the correlation between strain rate and seismicity in six tectonic settings representing typical plate boundary zones, diffuse plate boundary regions, and continental interiors. We analyzed and compared the spatial correlations between strain rate, seismicity, and seismic moment in these regions using the approach of Shen *et al.* (2007) and Zeng *et al.* (2018). We then investigated how correlations between strain rate and seismicity vary with time. We also explored the effects of seismic catalog completeness, cut-off magnitude, declustering, and model parameters. We show that the correlation between strain rates and seismicity is generally predictable by the regional strain rates: the higher the strain rates, the stronger the correlation.

Strain rates and Seismicity: Data, Method, and Results

The earthquake catalogs used in this study are from four sources: the historical and instrumental earthquake catalog for North China (-780 - 2015) (Cheng *et al.*, 2017), the earthquake catalogs (1568-2016) used for the 2018 USGS National Seismic Hazard Map (Mueller, 2019), the GEM Global Historical Earthquake Catalog (1000-1903) (Albini *et al.*, 2013; Albini *et al.*, 2014), and the ISC-GEM Global Instrumental Earthquake Catalog (1904-2015) (Storchak *et al.*, 2013; Storchak *et al.*, 2015; Giacomo *et al.*, 2018). All catalogs use the moment magnitude.

For strain rates, we used the results of the Global Strain Rate Model (GSRM v.2.1) (Kreemer *et al.*, 2014) for plate boundary zones and Kreemer *et al.* (2018) for the CEUS. GSRM v.2.1 is a global model of strain rates in the plate boundary zones constrained by horizontal geodetic site-velocities (Kreemer *et al.*, 2014). In the GSRM, significant transient motion due to postseismic deformation and slow slip events are excluded to represent "secular" or interseismic velocities. The resolution for GSRM v.2.1 is 0.1° longitude by 0.1° latitude in plate boundary zones. For intraplate North America, we used the strain rate model from Kreemer *et al.* (2018). The grid size of strain rate results is 0.5° by 0.5° with spatial resolution of ~100 km in the central and eastern United States (CEUS). The data used in Kreemer *et al.* (2018) are from continuous GPS networks, commercial and state networks, and networks installed to study the ionosphere, the troposphere, and surface subsidence.

In addition to the spatial distribution of earthquake epicenters, we considered the spatial distribution of seismic moment release. The seismic moment released by each earthquake is converted from its moment magnitude following Hanks and Kanamori (1979): $\log_{10} M_0 = 1.5\ M_w + 16.1$, where M_0 is the seismic moment in dyne-centimeter. As a first-order approximation, the moment released by each earthquake is assumed to be evenly distributed in a circular region centered at its epicenter with diameter equal to the empirical rupture length, estimated using the formula by Blaser *et al.* (2010).

We studied the spatial distribution of strain rate, earthquake, and seismic moment in six regions: California-Nevada, Japan, Anatolian, Tibetan Plateau, North China, and the CEUS, representing a spectrum of tectonic settings ranging from plate boundary zones to stable continental interiors. The first two regions are typical plate boundary zones. Anatolia and the Tibetan Plateau are diffuse plate boundary regions of continental collision. North China is an intraplate region of reactivated Archaean craton (Liu *et al.*, 2014), whereas the CEUS is a stable continental region with low strain rate.

The spatial distributions of seismicity, strain rate, and seismic moment of these regions are shown in Figure 1. For plate boundary zones and regions (California-Nevada and Japan, Figure 1a-d), most large earthquakes occurred and released seismic moment in areas of high strain rate. For diffuse plate boundary regions (Anatolia and the Tibetan Plateau), seismicity and moment release generally correlate with strain rates, but with noticeable exceptions – some large earthquakes occurred in the interior of regions where the strain rates are relatively low (Figure 1e-h). The correlations are more complicated for intraplate settings. In North China (Figure 1i-j), seismicity is concentrated in the circum-Ordos rift systems and the northern boundary of the North China block where strain rates are relatively high, but large earthquakes also occurred in regions of low strain rates (e.g., the 1556 Huaxian earthquake and the 1668 Tancheng earthquake). In the CEUS (Figure 1k-l), the correlation seems absent – most large historic earthquakes occurred in regions of the lowest strain rate.

Quantifying the strain rate-seismicity correlation

We followed the approach of Shen *et al.* (2007) and Zeng *et al.* (2018) to quantify the correlation between strain rate and seismicity and test the predicting power of strain rate for earthquake locations. For each seismic region, we gridded the region according to the spatial resolution of strain rate data and then sorted the grid cells by descending strain rate. Strain rate was then summed over the sorted cells to produce the cumulative value, plotted as a function of the fraction of covered area (Figure 2). If the strain rate distribution is random, its cumulative value would increase proportionally to the number of the cells (i.e., the fraction of covered area), and plot as a straight line. If the strain rate is localized in some areas, then the plot would be a concave curve, with the highest strain rate areas to the left of the plot. The curve would be more concave if the strain rate is more concentrated. In the plots, the cumulative strain rate and the cumulative number of the sorted cells (covered area) are normalized to unity for comparison.

The normalized cumulative number of earthquakes was counted from the cells of descending strain rates and plotted together with the cumulative strain rates (Figure 2). Again, if earthquake distribution is random, the cumulative earthquakes would plot as a straight line (staircases in practice because of finite numbers of earthquakes in each cell), i.e., they increase proportionally with the fraction of covered area. If seismicity is concentrated in areas of high strain rate, then the normalized cumulative earthquake counts would plot closely to the normalized cumulative strain rate values (we call these seismicity and strain rate curves, for convenience) (Figure 2). This plot, a "success diagram", illustrates how "successfully" strain rate predicts the locations of earthquakes. This is a flipped version of the Molchan error diagram used to test earthquake predictions (Molchan and Kagan, 1992; Zechar and Jordan, 2008).

Figure 3 compares the success diagrams for three regions: California-Nevada (plate boundary zone), North China (active continental interior), and the CEUS (stable continent). In California-Nevada, both strain rates and large earthquakes ($M \geq 6.5$) are highly concentrated, and their spatial correlation is strong. Thus, strain rate in this region is a good spatial predictor of large earthquakes. In North China, strain rates are relatively localized and have a good spatial correlation with large earthquakes. In the CEUS, strain rates are somewhat concentrated in some areas but not correlated to earthquakes – the seismicity curve is close to but slightly below the diagonal line, indicating that earthquakes are nearly randomly distributed in space, and more earthquakes occurred in areas of relatively lower strain rates. In this case, strain rate has no use as an indicator of future earthquake locations.

We then compared the correlations between strain rates, seismicity, and moment release in each region. We used catalogs from previous studies and chose time span and cut-off magnitude for complete records (Huang *et al.*, 1994; Albini *et al.*, 2013; Petersen *et al.*, 2020).

The normalized cumulative moment-release curve (moment curve for short) was constructed the same way as the seismic curve: summed from cells sorted in order of descending strain rate. In California-Nevada and Japan, good spatial correlations are found between strain rate, seismicity, and seismic moment release (Figure 4a, b). In Anatolia, the seismicity and moment curves match with each other, but they are slightly below the strain rate curve (Figure 4c). This deviation may be caused by the lack of $M \geq 7$ earthquakes in the regions of medium strain rates in central and western Anatolian peninsula (Figure 1e). In the Tibetan Plateau, strain rate has a good spatial correlation with large earthquakes ($M \geq 7$) but is poorly correlated with seismic moment release (Figure 4d), perhaps because the stored seismic moment is not totally released in the short period of the catalog.

North China is similar to the Tibetan Plateau where strain rate correlates well with seismicity but poorly with seismic moment release (Figure 4e). North China has a lower average strain rate than Anatolia or the Tibetan Plateau, so the recurrence intervals for large earthquakes are longer, and the seismic moment curve can be strongly influenced by a few large earthquakes in the catalog. For example, the 1668 *M*8.4 Tancheng earthquake (Figure 1j), one of the largest earthquakes in North China (Liu *et al.*, 2014), occurred in an area of low strain rate (Figure 1i). For the CEUS, we used a longer seismic catalog than that in Kreemer *et al.* (2018) and obtained similar results: the correlation between strain rate, seismicity, and seismic moment is poor or absent (Figure 4f). The seismicity curve is close to the diagonal line (Figure 4f), suggesting that the $M \geq 5$ earthquakes in the CEUS are close to a random distribution and not correlated with strain rate. Moreover, the seismic moment is mainly released in regions of low strain rate (Figure 4f), where the 1811-1812 New Madrid earthquakes and the 1886 Charleston earthquake occurred. We also analyzed the $M \geq 5$ background seismicity and smaller modern seismicity (*M*

≥ 2.5); the results are similar (Figure 5). The factors for the significant difference between strain rate, seismicity, and seismic moment in the CEUS are discussed later.

We can further quantify the spatial concentration of strain rate and its correlation with seismicity using the area skill score (Zechar and Jordan, 2008), which is the fractional area below the corresponding strain curve (or the staircase for earthquake counts) in the success diagram (Figures 3-5). If strain rate is randomly distributed in a region, the strain rate curve follows the diagonal line, therefore the area skill score is 0.5. When strain rate is highly localized, such as in California-Nevada or Japan, the strain curves are strongly concave, and their area skill scores are much greater than 0.5. The area skill score of the seismicity (or seismic moment) curves, which are based on strain rates, characterizes how concentrated seismicity (or seismic moment) is in high strain-rate areas. If a seismic curve has a high area skill score, it means that strain rate is a good predictor for earthquakes. A less than 0.5 score means more earthquakes occurred in areas of lower strain rate. In other words, strain rate as a spatial earthquake predictor would fare worse than random guessing. The same is true for the moment curves in these figures.

The results of area skill scores for the six studied regions are shown in Figure 4 and Table 1. Except for the CEUS, all other regions have area skill scores > 0.5 for seismicity, with the highest value (0.85) in California-Nevada. In these regions, strain rate as a predictor for earthquakes would fare better than random guessing. For the CEUS, the area skill score for the seismicity (staircase) is lower than 0.5 (Figure 5), meaning that more earthquakes occurred in lower strain rate areas. Thus, using strain rate as a spatial predictor of earthquakes would fare worse than random guessing in the CEUS.

The correlation between strain rate and seismicity (or seismic moment) can be quantified by the closeness between the strain rate curve and the corresponding seismicity (or moment) curve for a region. We use ΔA_{eq} to represent the fractional area between the strain rate curve and seismicity curve, and ΔA_m for the fractional area between the strain rate and seismic moment curves (Table 1). Both ΔA_{eq} and ΔA_m are small for plate boundary zones (California-Nevada and Japan), indicating strong correlation between strain rate and seismicity (seismic moment). North China has low ΔA_{eq} but large ΔA_m, indicating that strain rate is a good spatial indicator of seismicity but poor indicator for moment release, because several large earthquakes occurred in areas of low strain rates (Figure 1i-j). The CEUS has large ΔA_{eq} and ΔA_m, indicating that strain rate is a poor predictor for either earthquakes or seismic moment release. We also found that ΔA_m is negatively correlated with strain rate (Figure 6), which means poorer correlations between strain rate and moment release in lower strain rate regions.

Temporal variations of strain rate-seismicity correlation

Regional seismicity rate varies with time (Omori, 1894; Kagan and Jackson, 1991) and thus would affect strain rate-seismicity correlation. A major cause of the temporal variation is earthquake clustering (aftershocks and foreshocks), but even background seismicity rate can change in time (Zhuang *et al.*, 2005; Llenos and Michael, 2013; Chen *et al.*, 2021). We analyzed the temporal variations of the correlation between strain rate and relatively small earthquakes in California-Nevada, North China, and the CEUS. Both the original catalogs and declustered catalogs were used. We obtained the declustered catalogs using the nearest-neighbor method (Baiesi and Paczuski, 2004; Zaliapin *et al.*, 2008; Chen *et al.*, 2021; Chen and Liu, 2023). In California and Nevada, the correlation between strain rate and seismicity varies with time for both background earthquakes and all events with the same trend (Figure 7a-b): poorer correlations from 1933 to the 1980s and better correlations from the 1980s to 2016. This trend of temporal variation is similar to the results of Zeng *et al.* (2018) based on background earthquakes. In North China (Figure 7c), the seismicity curves for total events are above the strain rate curve in the 1970s and 1980s, because most events during that time were aftershocks of the 1976 Great Tangshan earthquake (Chen *et al.*, 2021), and both the mainshock and its aftershocks were concentrated in areas of high strain rate (Figure 1i-j). As time passed, aftershock activity decayed and background earthquakes, many in areas of relatively low strain rate, become relatively dominant. Therefore, the correlation between strain rate and seismicity worsens. A similar trend is found for background seismicity (Figure 7d). After 2000, most events in North China are background earthquakes and they are diffusely distributed. In the CEUS, some temporal variations exist (Figure 7e-f). The seismicity curves are below the diagonal line (for spatially random distribution) and move downward as time passed, indicating even more small events occurred in areas of low strain rate. These trends of the temporal variations of strain rate-seismicity correlation do not change with different lengths of time windows used in constructing these curves (Figure S1).

Over a longer time, seismicity rate may change between relatively active (clustered) periods and relatively inactive (quiescent) periods (Figure 8a). These temporal variations have been described as the Devil's staircases (Chen *et al.*, 2020) or supercycles (Sieh *et al.*, 2008; Goldfinger *et al.*, 2013; Salditch *et al.*, 2019). For North China, the complete records of $M \geq 6$ earthquakes show an active period between 1600 and 1750, followed by a relatively quiescent period (1750-1900), then another active period since 1900 (Figure 8a). We compared the seismicity curves in these periods with the strain rate curves, and the results show that the seismicity curves for the two active periods match the strain rate curve well (Figure 8b), but the seismicity curve for the quiescent period is significantly below the strain rate curve and close to spatially random distribution (Figure 8b). Similar results are found in California-Nevada (Zeng *et al.*, 2018). Therefore, good correlations between strain rate and seismicity may correspond to periods of relatively active seismicity, while poor correlations may correspond to relatively quiescent periods of seismicity.

Discussion

The past few decades have seen rapid development and applications of space-based geodesy, which has been providing unprecedented details of present-day crustal deformation. The geodetic strain rates indicate where and how fast strain is accumulating, therefore where future earthquakes may occur. However, for strain rate to be a useful spatial predictor of earthquakes, their spatial distributions need to be closely correlated, yet such correlations seem to vary significantly in different regions (Kreemer *et al.*, 2018; Zeng *et al.*, 2018; Chen *et al.*, 2021).

In this study, we systematically characterized the correlation between strain rate, seismicity, and seismic moment in different tectonic settings. We found that the strain rate-seismicity correlation is complex (Figures 1, 3-4) and may be characterized by the regional mean strain rates (Table 1). In typical plate boundary zones (e.g., California and Japan), strain rates are generally high and concentrated at major fault zones where most large earthquakes occur. Fast tectonic loading in these regions also means short interseismic intervals, hence more representative earthquake catalogs. Therefore, strain rate correlates well with seismicity and seismic moment release. In this case, strain rate is a good spatial predictor of seismicity, as previously suggested (Shen *et al.*, 2007; Zeng *et al.*, 2018). In broadly diffuse plate boundary regions (e.g., the Tibetan Plateau) and boundaries of microplates (e.g., Anatolia), correlations between strain rate and seismicity are still good, but the predicting power of strain rate for earthquakes is not as good as in typical plate boundary zones (Figure 1, 4), because the strain rate distribution is more diffuse, and many earthquakes occur in areas of median or low strain rates. In continental interiors, strain rate is relatively low and its spatial correlation with seismicity is generally poor. North China is an end-member case with active fault systems and relatively high strain rate (Liu and Wang, 2012; Chen *et al.*, 2021), strain rate has a reasonably good correlation with seismicity but not seismic moment release (Figure 1, 4), because some large historic earthquakes occurred in areas of low strain rates. The CEUS represent another end-member case: stable plate interiors where strain rate is extremely low and its correlation with seismicity is poor or absent (Figure 1, 5), as suggested by previous studies (Calais *et al.*, 2016; Kreemer *et al.*, 2018). In such settings, strain rate cannot be used as a useful spatial predictor of seismicity.

The contrast between North China and the CEUS also highlights the complexity of strain rate and seismicity data in continental interiors. The measured strain rates may include non-tectonic components, and low strain rates in these regions means long recurrence intervals for large earthquakes. Earthquake records in intraplate regions are often too short to provide representative long-term spatiotemporal patterns (Liu and Stein, 2016). The relatively good strain rate-seismicity correlation in North China may indicate that the observed geodetic strain rate reflects the long-term interseismic loading. However, the long-lasting aftershocks and postseismic deformation of the 1966 Xingtai earthquake and the 1976 Tangshan earthquake in North China (Liu and Wang, 2012; Liu *et al.*, 2014; Chen *et al.*, 2021) may cause an overestimation of the goodness of the correlation between strain rate and seismicity. In contrast, geodetic strain rates in the CEUS are dominated by glacial isostatic adjustment (GIA), which partially explains the poor or no correlation between strain rate and seismicity (Figure 4f) (Calais *et al.*, 2006; Kreemer *et al.*, 2018). Based on the lack of strain rate-seismicity correlation in the CEUS, Kreemer *et al.* (2018) argued that "intraplate seismicity does not reflect the release of geodetic strain, and the largest, GIA-controlled, strain rate does not load faults, except perhaps in zones of weakness such as continental margins."

Geodetic strain rate in most tectonically active regions reflects mainly long-term steady tectonic loading, and is therefore correlated to seismicity, with noticeable exceptions in stable continents like the CEUS. Even in diffuse plate boundary regions and active continental interiors, strain rate has some predicting power for future locations of earthquakes (or seismic moment release), and would fare better than random guessing. If current strain rate fields reflect long-term interseismic loading, then they should be correlated with long-term seismic moment release. Therefore, deviations between the strain rate curve and the seismic moment curve in a short-term record may offer information about where strain is insufficiently released (Yin *et al.*, 2023). For example, in North China (Figure 4e), future large earthquakes may be more likely to occur in regions of medium strain rates because the stored energy there has not been sufficiently released in the past 400 years.

While we discussed six tectonic regions as single units, within each region, especially the regions of diffuse plate boundary zones or continental interiors, the correlation between strain rate, seismicity, and seismic moment release may vary significantly. For example, in the western part of North China, both seismicity and moment release concentrate in high strain rate areas (Figure S2a-b), but in the eastern part of North China, strain rate correlates with seismicity but not with moment release (Figure S2c-d). Within the North China Plain, strain rate correlates with neither seismicity nor moment release (Figure S2e-f). Such variations are related to strain rate: the correlation is better in higher strain rate regions but poorer in lower strain rate regions (Figure 6 and Figure S3). Thus, in intraplate regions large earthquakes could occur in subregions of low strain rate.

The correlation between strain rate and seismicity also varies with time (Figures 7-8) and needs to be considered in hazard assessment. Hazard maps usually estimate seismic hazard in the next 50 years (Petersen *et al.*, 2014; Petersen *et al.*, 2020). However, in a 50-year window, the spatial distributions of seismicity can vary significantly (Figure 7). This effect is minor in plate boundary zones, because the recurrence intervals there are relatively short and most events occur in areas of high strain rates in all periods (Figure 7a-b). In intraplate regions like North China, because of long recurrence intervals, spatial distributions of seismicity can vary significantly in different periods (Figure 7c-d, 8). In an active period, earthquakes tend to concentrate in areas of high strain rate, but in a relatively quiescent period, earthquake distribution is diffuse and closer to be random. The spatial distributions of small earthquakes seem to have clear trend of temporal variations (Figure 7), which has been related to different phases of regional stress accumulation and release (Zeng *et al.*, 2018). These temporal variations and trends may be used to tell if a region is entering a more active or a relatively quiescent period of seismicity, as suggested by Zeng *et al.* (2018).

Conclusions

We have systematically studied the correlation between strain rate and seismicity in different tectonic settings, and evaluated how good strain rate is as a spatial indictor of earthquakes and moment release in these regions. The strain rate-seismicity correlation is strong in plate boundary zones where strain rate is high and localized at a few major fault zones. In this case strain rate is a good spatial predictor of earthquakes and seismic moment release. In diffuse plate boundary regions and tectonically active continents, strain rates are relatively high and generally correlated with seismicity. Strain rate could be a useful spatial predictor of seismicity, and deviation of cumulative moment release from cumulative strain may provide information of where large earthquakes may occur in the future. However, in stable continents such as the CEUS, strain rates are low and may be dominated by non-tectonic strain, thus the correlation between strain rate and seismicity is poor or absent. In this case strain rate cannot be used as a spatial indictor of seismicity; it would fare worse than random guessing.

The strain rate-seismicity correlation is time-dependent, because the spatiotemporal distribution of earthquakes, including background seismicity, are found to change with time. Better correlations are found in seismically active periods and poorer in relatively quiescent periods. If the trends of the temporal change can be clearly established, they may indicate if a given region is entering an active period of seismic activity, which can be useful for hazard assessment.

Data and Resources

The China fault data is available at https://data.earthquake.cn/datashare/report.shtml?PAGEID=datasourcelist&dt=ff8080826e16801d016eb119cb350006 (last accessed October, 2022) from China Earthquake Networks Center and National Earthquake Data Center.

Acknowledgement

We are grateful to Seth Stein for his helpful review and editing, and to the AE and an anonymous reviewer for their constructive comments. This work is part of Y. Chen's Ph.D. research. M. Liu acknowledges support from NSF (grants 1519980 and 2013656).

References

Albini, P., R. Musson, A. Gomez Capera, M. Locati, A. Rovida, M. Stucchi, and D. Viganò (2013). Global historical earthquake archive and catalogue (1000-1903).

Albini, P., R. M. Musson, A. Rovida, M. Locati, A. A. Gomez Capera, and D. Viganò (2014). The global earthquake history, *Earthquake Spectra* **30** 607-624.

Baiesi, M., and M. Paczuski (2004). Scale-free networks of earthquakes and aftershocks, *Physical Review E* **69** 066106.

Blaser, L., F. Krüger, M. Ohrnberger, and F. Scherbaum (2010). Scaling relations of earthquake source parameter estimates with special focus on subduction environment, *Bulletin of the Seismological Society of America* **100** 2914-2926.

Calais, E., T. Camelbeeck, S. Stein, M. Liu, and T. Craig (2016). A new paradigm for large earthquakes in stable continental plate interiors, *Geophysical Research Letters* **43**.

Calais, E., J. Han, C. DeMets, and J. Nocquet (2006). Deformation of the North American plate interior from a decade of continuous GPS measurements, *Journal of geophysical research: solid earth* **111**.

Chen, Y., and M. Liu (2023). Long-Lived Aftershocks in the New Madrid seismic Zone and the Rest of Stable North America, *Journal of Geophysical Research: Solid Earth* **128** e2023JB026482.

Chen, Y., M. Liu, and G. Luo (2020). Complex Temporal Patterns of Large Earthquakes: Devil's Staircases, *Bulletin of the Seismological Society of America* **110** 1064-1076.

Chen, Y., M. Liu, and H. Wang (2021). Aftershocks and background seismicity in Tangshan and the rest of North China, *Journal of Geophysical Research: Solid Earth* e2020JB021395.

Cheng, J., Y. Rong, H. Magistrale, G. Chen, and X. Xu (2017). An Mw-based historical earthquake catalog for Mainland China, *Bulletin of the Seismological Society of America* **107** 2490-2500.

Giacomo, D. D., E. R. Engdahl, and D. A. Storchak (2018). The ISC-GEM Earthquake Catalogue (1904–2014): status after the Extension Project, *Earth System Science Data* **10** 1877-1899.

Goldfinger, C., Y. Ikeda, R. S. Yeats, and J. Ren (2013). Superquakes and supercycles, *Seismological Research Letters* **84** 24-32.

Hanks, T. C., and H. Kanamori (1979). A moment magnitude scale, *Journal of Geophysical Research: Solid Earth* **84** 2348-2350.

Huang, W.-Q., W.-X. Li, and X.-F. Cao (1994). Research on the completeness of earthquake data in the Chinese mainland (I)—North China, *Acta Seismologica Sinica* **7** 351-359.

Kagan, Y. Y., and D. D. Jackson (1991). Long-term earthquake clustering, *Geophysical Journal International* **104** 117-133.

Kreemer, C., G. Blewitt, and E. C. Klein (2014). A geodetic plate motion and Global Strain Rate Model, *Geochemistry, Geophysics, Geosystems* **15** 3849-3889.

Kreemer, C., W. C. Hammond, and G. Blewitt (2018). A robust estimation of the 3-D intraplate deformation of the North American plate from GPS, *Journal of Geophysical Research: Solid Earth* **123** 4388-4412.

Kreemer, C., W. E. Holt, and A. J. Haines (2002). The global moment rate distribution within plate boundary zones, *Plate boundary zones* **30** 173-190.

Kreemer, C., and Z. M. Young (2022). Crustal Strain Rates in the Western United States and Their Relationship with Earthquake Rates, *Seismological Research Letters* **93** 2990-3008.

Liu, M., and S. Stein (2016). Mid-continental earthquakes: Spatiotemporal occurrences, causes, and hazards, *Earth-Science Reviews* **162** 364-386.

Liu, M., and H. Wang (2012). Roaming earthquakes in China highlight midcontinental hazards, *Eos, Transactions American Geophysical Union* **93** 453-454.

Liu, M., H. Wang, J. Ye, and J. Cheng (2014). Intraplate earthquakes in North China, in *Intraplate Earthquakes* P. Talwani (Editor), Cambridge University Press, New York, 97-125.

Llenos, A. L., and A. J. Michael (2013). Modeling earthquake rate changes in Oklahoma and Arkansas: Possible signatures of induced seismicity, *Bulletin of the Seismological Society of America* **103** 2850-2861.

Molchan, G., and Y. Y. Kagan (1992). Earthquake prediction and its optimization, *Journal of Geophysical Research: Solid Earth* **97** 4823-4838.

Mueller, C. S. (2019). Earthquake catalogs for the USGS national seismic hazard maps, *Seismological Research Letters* **90** 251-261.

Omori, F. (1894). On the after-shocks of earthquakes, The University.

Petersen, M. D., M. P. Moschetti, P. M. Powers, C. S. Mueller, K. M. Haller, A. D. Frankel, Y. Zeng, S. Rezaeian, S. C. Harmsen, O. S. Boyd, N. Field, R. Chen, K. S. Rukstales, N. Luco, R. L. Wheeler, R. A. Williams, and A. H. Olsen (2014). Documentation for the 2014 update of the United States national seismic hazard maps, Geological Survey (US).

Petersen, M. D., A. M. Shumway, P. M. Powers, C. S. Mueller, M. P. Moschetti, A. D. Frankel, S. Rezaeian, D. E. McNamara, N. Luco, and O. S. Boyd (2020). The 2018 update of the US National Seismic Hazard Model: Overview of model and implications, *Earthquake Spectra* **36** 5-41.

Salditch, L., S. Stein, J. Neely, B. D. Spencer, E. M. Brooks, A. Agnon, and M. Liu (2019). Earthquake supercycles and Long-Term Fault Memory, *Tectonophysics* 228289.

Shen, Z.-K., D. D. Jackson, and Y. Y. Kagan (2007). Implications of Geodetic Strain Rate for Future Earthquakes, with a Five-Year Forecast of M5 Earthquakes in Southern California, *Seismological Research Letters* **78** 116-120.

Sieh, K., D. H. Natawidjaja, A. J. Meltzner, C.-C. Shen, H. Cheng, K.-S. Li, B. W. Suwargadi, J. Galetzka, B. Philibosian, and R. L. Edwards (2008). Earthquake supercycles inferred from sea-level changes recorded in the corals of west Sumatra, *Science* **322** 1674-1678.

Stevens, V., and J. Avouac (2021). On the relationship between strain rate and seismicity in the India–Asia collision zone: implications for probabilistic seismic hazard, *Geophysical Journal International* **226** 220-245.

Storchak, D. A., D. Di Giacomo, I. Bondár, E. R. Engdahl, J. Harris, W. H. Lee, A. Villaseñor, and P. Bormann (2013). Public release of the ISC–GEM global instrumental earthquake catalogue (1900–2009), *Seismological Research Letters* **84** 810-815.

Storchak, D. A., D. Di Giacomo, E. Engdahl, J. Harris, I. Bondár, W. H. Lee, P. Bormann, and A. Villaseñor (2015). The ISC-GEM global instrumental earthquake catalogue (1900–2009): introduction, *Physics of the Earth and Planetary Interiors* **239** 48-63.

Styron, R., and M. Pagani (2020). The GEM global active faults database, *Earthquake Spectra* **36** 160-180.

Tarayoun, A., S. Mazzotti, M. Craymer, and J. Henton (2018). Structural inheritance control on intraplate present-day deformation: GPS strain rate variations in the Saint Lawrence Valley, eastern Canada, *Journal of Geophysical Research: Solid Earth* **123** 7004-7020.

Wu, Y., Z. Jiang, Y. Pang, and C. Chen (2021). Statistical Correlation of Seismicity and Geodetic Strain Rate in the Chinese Mainland, *Seismological Research Letters* **93** 268-276.

Yin, L., G. Luo, and M. Liu (2023). Moment budget and seismic potential of the Xianshuihe-Xiaojiang fault system, southeastern Tibetan Plateau, *Tectonophysics* 229935.

Zaliapin, I., A. Gabrielov, V. Keilis-Borok, and H. Wong (2008). Clustering analysis of seismicity and aftershock identification, *Physical review letters* **101** 018501.

Zechar, J. D., and T. H. Jordan (2008). Testing alarm-based earthquake predictions, *Geophysical Journal International* **172** 715-724.

Zeng, Y., M. D. Petersen, and Z. K. Shen (2018). Earthquake potential in California-Nevada implied by correlation of strain rate and seismicity, *Geophysical Research Letters* **45** 1778-1785.

Zhuang, J., C. P. Chang, Y. Ogata, and Y. I. Chen (2005). A study on the background and clustering seismicity in the Taiwan region by using point process models, *Journal of Geophysical Research: Solid Earth* **110**.

Full mailing address for each author

1. Yuxuan Chen

Mailling address: 129 Luoyu Road, School of Geodesy and Geomatics, Wuhan University, Wuhan 430079, China

Email: yc2023@whu.edu.cn

2. Mian Liu

Mailling address: 101 Geological Sciences Building, Dept. of Geological Sciences, University of Missouri, Columbia, MO 65211, USA.

Email: lium@missouri.edu

Tables

Table 1. Quantification of strain rate-seismicity correlations shown in Figures 1 and 4

Region	Mean strain rate (10^{-9}/year)	Uncertainty range of mean strain rate	Time	Magnitude	Area skill score of strain rate (Earthquake)	ΔA_{eq}	ΔA_m
California	61.0	58.7-64.4	1852-2016	$M \geq 6.5$	0.85 (0.85)	0.025	0.028
Japan	184.0	182.1-186.2	1586-2015	$M \geq 7$	0.73 (0.72)	0.023	0.022
Anatolia	64.6	62.2-67.3	1045-2015	$M \geq 7$	0.76 (0.69)	0.077	0.057
Tibet	28.0	25.7-31.8	1786-2015	$M \geq 7$	0.73 (0.75)	0.027	0.094
North China	4.8	2.7-8.9	1604-2015	$M \geq 6$	0.75 (0.74)	0.021	0.111
CEUS	1.1	0.5-2.3	1568-2016	$M \geq 5$	0.67 (0.44)	0.225	0.510

List of Figure Captions

Figure 1. **(a)** Spatial distribution of seismicity (circles, $M \geq 6$, 1769-2016) and strain rate (color contours) in California-Nevada. **(b)** Spatial distribution of seismicity (circles, $M \geq 6$, 1769-2016) and the seismic moment release (color contours) in California-Nevada. **(c-d)** Same as (a-b) but for seismicity ($M \geq 7$, 1096-2015), strain rate, and seismic moment in Japan. **(e-f)** Same as (a-b) but for seismicity ($M \geq 6$, 1045-2015), strain rate, and seismic moment in Anatolia. **(g-h)** Same as (a-b) but for seismicity ($M \geq 6$, 1117-2015), strain rate, and seismic moment in Tibet. HYF: Haiyuan fault; XFS: Xianshuihe fault system. **(i-j)** Same as (a-b) but for seismicity ($M \geq 6$, -780-2015), strain rate, and seismic moment in North China. ZPFS: Zhangjiakou-Penglai fault system. **(k-l)** Same as (a-b) but for seismicity ($M \geq 5$, 1568-2016), strain rate, and seismic moment in the CEUS. The fault data are from the GEM global active faults database (Styron and Pagani, 2020) and China Earthquake Networks Center and National Earthquake Data Center (see Data and Resources).

Figure 2. Illustration of the procedure that transforms strain rate and earthquake data to the "success diagram". The grid cells are sorted by descending strain rate values ($sr_1, sr_2, \dots, sr_n$), so the cumulative value of strain rate increases with the number of the cells (fraction of covered area) as a concave curve. The numbers of earthquakes that occurred in these cells are $eq_1, eq_2, \dots, eq_n$. If earthquakes are randomly distributed in space as shown here, the cumulative earthquakes increase linearly with the number of cells.

Figure 3. Comparison between strain rate and seismicity in different tectonic settings. Curves: cumulative strain rate; staircases: cumulative earthquake count. The method is explained in the text and illustrated in Figure 2. The concave strain rate curves for California-Nevada and North

China indicate strain rate concentration, and their closeness to the cumulative earthquake counts (staircases) indicate strong correlations between strain rate and earthquakes. In the CEUS, the cumulative counts plotted close to the diagonal line, showing that large earthquakes (M ≥ 5) are nearly randomly distributed in space.

Figure 4. Comparison of correlations between strain rate, seismicity, and seismic moment in different tectonic settings. Cumulative strain rate, earthquake count, and seismic moment are plotted against the fraction of covered area sorted by descending strain rates, with the highest strain rate areas located to the left of the horizontal axis. The scores in the legend are the area skill scores explained in the text. The diagonal line indicates random distribution in space (area skill score = 0.5).

Figure 5. Comparison of the correlations between strain rate and seismicity in the CEUS for **(a)** all events, **(b)** background events of $M \geq 5$ between 1811 and 2016. **(c)**-**(d)** Same as (a)-(b) but for $M \geq 2.5$ events between 1980 and 2016. The background seismicity is obtained by declustering the catalog using the nearest-neighbor method.

Figure 6. Relationship between strain rate and ΔA_m (the fractional area between the strain rate curve and seismic moment curve) based on the results in Table 1. Regions with higher strain rate have smaller values of ΔA_m, which indicates better correlation between strain rate and seismic moment release in higher strain rate regions.

Figure 7. Temporal variations of strain rate-seismicity correlation in California and Nevada for **(a)** all $M \geq 4$ events or **(b)** $M \geq 4$ background earthquakes. The cumulative earthquakes are counted within a 10-year window that moves in 2-year steps from 1933 to 2016. **(c-d)** Same for (a-b), but for $M \geq 4$ earthquakes in North China from 1970 to 2015. **(e-f)** Same for (a-b), but for $M \geq 2.5$ earthquakes in the CEUS from 1980 to 2016. The color bar shows the midyear of the moving 10-year windows used to calculate the cumulative earthquake counts. The thick black curve is the cumulative strain rate. The diagonal line indicates spatially random distribution.

Figure 8. (a) Temporal pattern of $M \geq 6$ earthquakes ($M \geq 6.5$ for inset) in North China with two active periods (1600-1750 and 1900-2015) separated by a relatively quiescent period (1750-1900). **(b)** Comparison of correlations between strain rate (red curve) and seismicity in these three periods. The diagonal line indicates a random distribution of earthquakes.

Figures

541

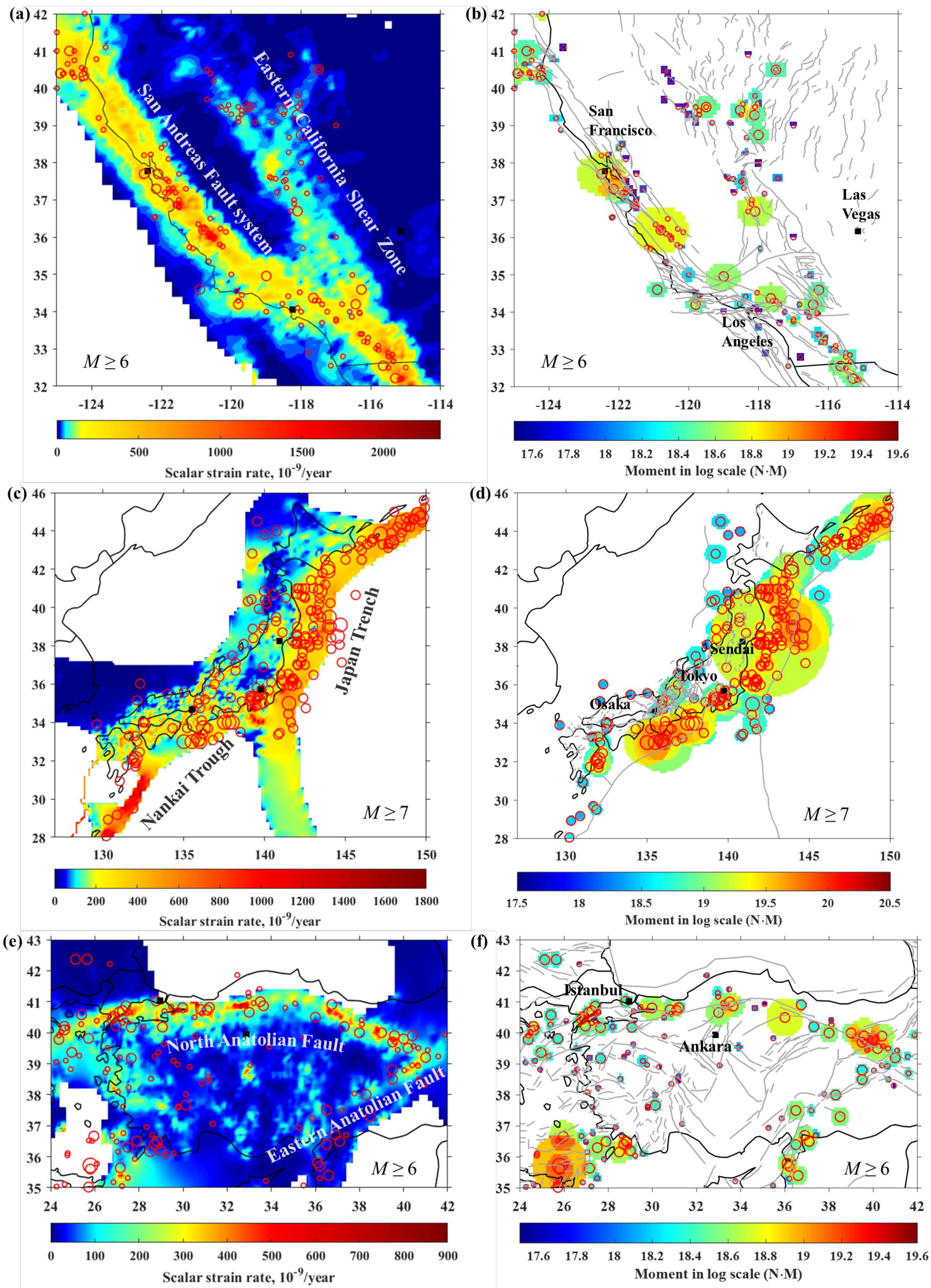

(a)
San Andreas Fault system
Eastern California Shear Zone
M ≥ 6
Scalar strain rate, 10^-9/year
(b)
San Francisco
Las Vegas
Los Angeles
M ≥ 6
Moment in log scale (N·M)
(c)
Japan Trench
Nankai Trough
M ≥ 7
Scalar strain rate, 10^-9/year
(d)
Sendai
Tokyo
Osaka
M ≥ 7
Moment in log scale (N·M)
(e)
North Anatolian Fault
Eastern Anatolian Fault
M ≥ 6
Scalar strain rate, 10^-9/year
(f)
Istanbul
Ankara
M ≥ 6
Moment in log scale (N·M)

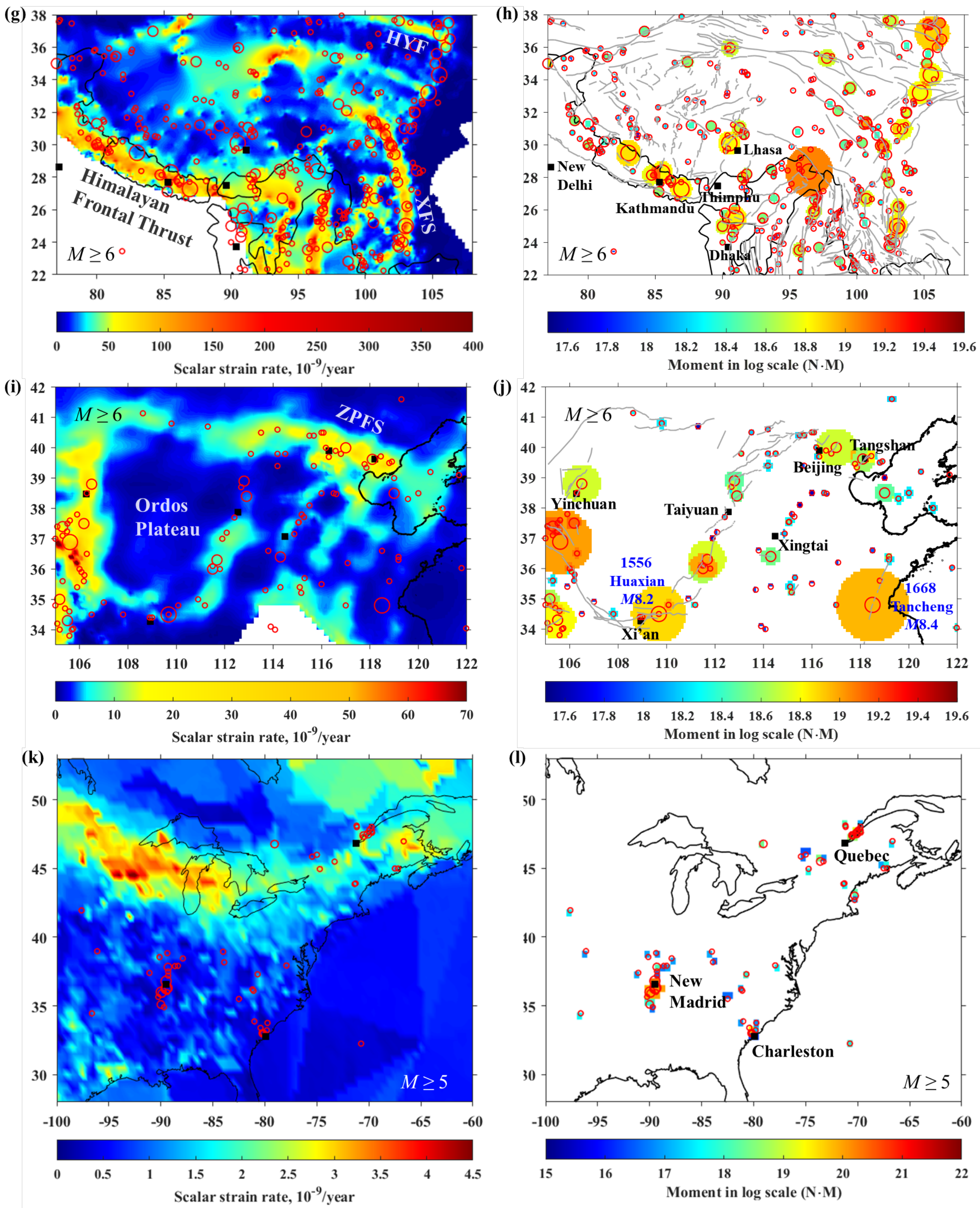

Figure 1. (a) Spatial distribution of seismicity (circles, $M \geq 6$, 1769-2016) and strain rate (color contours) in California-Nevada. **(b)** Spatial distribution of seismicity (circles, $M \geq 6$, 1769-2016)

and the seismic moment release (color contours) in California-Nevada. **(c-d)** Same as (a-b) but for seismicity ($M \geq 7$, 1096-2015), strain rate, and seismic moment in Japan. **(e-f)** Same as (a-b) but for seismicity ($M \geq 6$, 1045-2015), strain rate, and seismic moment in Anatolia. **(g-h)** Same as (a-b) but for seismicity ($M \geq 6$, 1117-2015), strain rate, and seismic moment in Tibet. HYF: Haiyuan fault; XFS: Xianshuihe fault system. **(i-j)** Same as (a-b) but for seismicity ($M \geq 6$, -780-2015), strain rate, and seismic moment in North China. ZPFS: Zhangjiakou-Penglai fault system. **(k-l)** Same as (a-b) but for seismicity ($M \geq 5$, 1568-2016), strain rate, and seismic moment in the CEUS. The fault data are from the GEM global active faults database (Styron and Pagani, 2020) and China Earthquake Networks Center and National Earthquake Data Center (see Data and Resources).

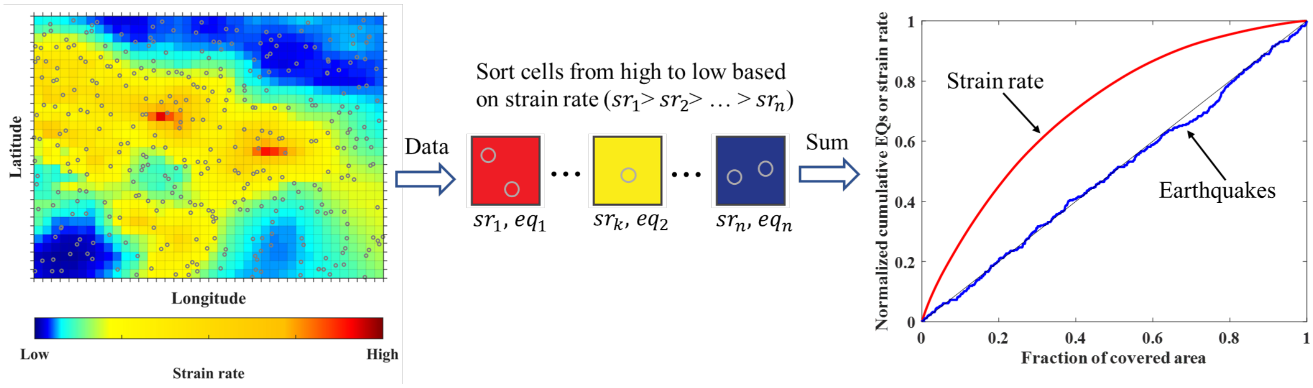

Figure 2. Illustration of the procedure that transforms strain rate and earthquake data to the "success diagram". The grid cells are sorted by descending strain rate values ($sr_1, sr_2, \dots, sr_n$), so the cumulative value of strain rate increases with the number of the cells (fraction of covered area) as a concave curve. The numbers of earthquakes that occurred in these cells are $eq_1, eq_2, \dots, eq_n$. If earthquakes are randomly distributed in space as shown here, the cumulative earthquakes increase linearly with the number of cells.

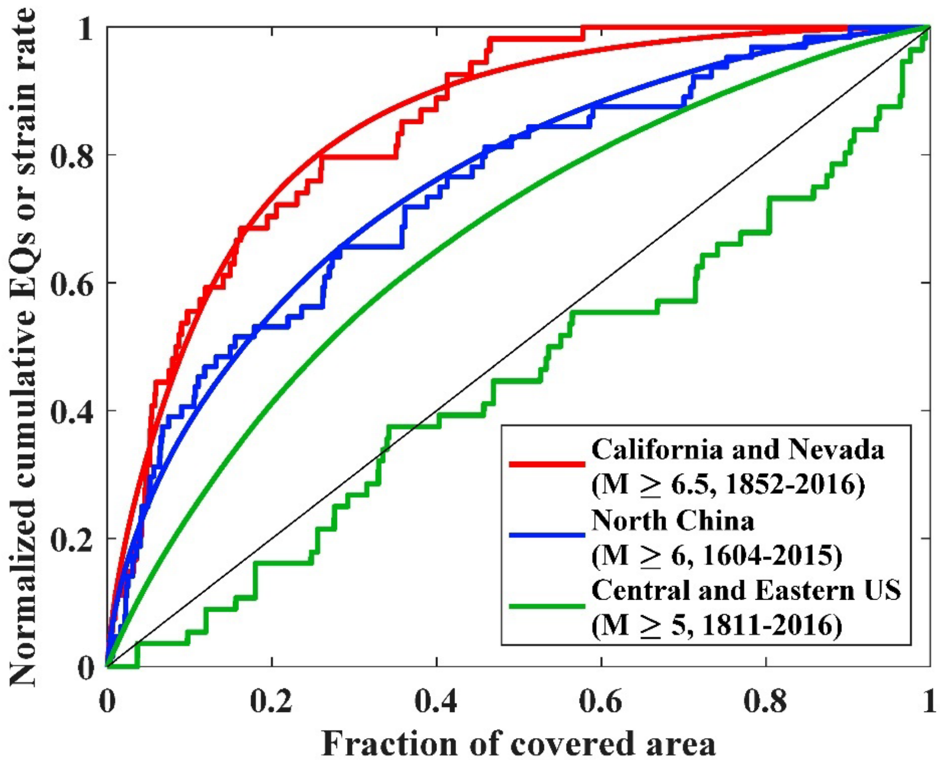

Figure 3. Comparison between strain rate and seismicity in different tectonic settings. Curves: cumulative strain rate; staircases: cumulative earthquake count. The method is explained in the text and illustrated in Figure 2. The concave strain rate curves for California-Nevada and North China indicate strain rate concentration, and their closeness to the cumulative earthquake counts (staircases) indicate strong correlations between strain rate and earthquakes. In the CEUS, the cumulative counts plotted close to the diagonal line, showing that large earthquakes ($M \geq 5$) are nearly randomly distributed in space.

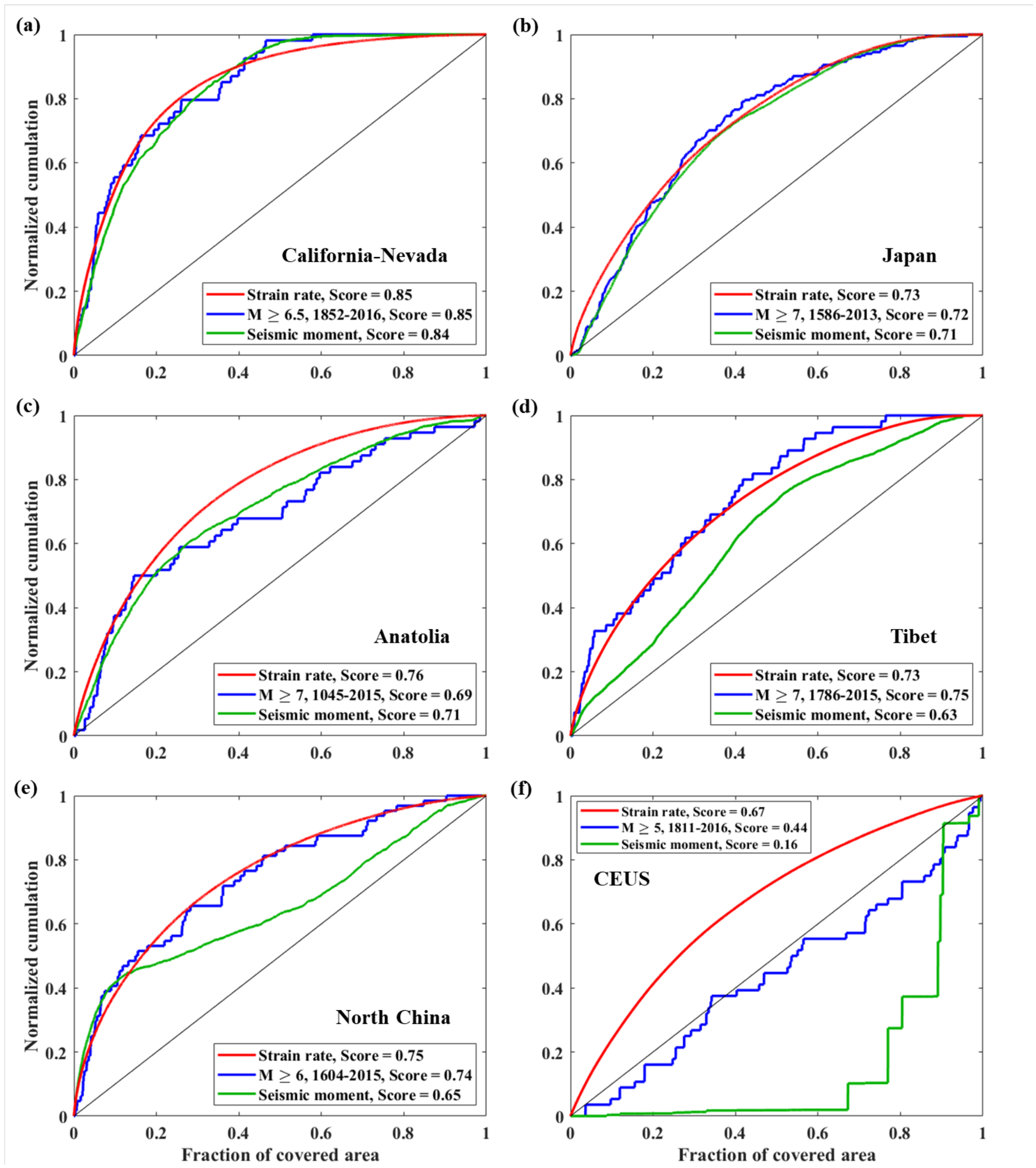

Figure 4. Comparison of correlations between strain rate, seismicity, and seismic moment in different tectonic settings. Cumulative strain rate, earthquake count, and seismic moment are plotted against the fraction of covered area sorted by descending strain rates, with the highest strain rate areas located to the left of the horizontal axis. The scores in the legend are the area

skill scores explained in the text. The diagonal line indicates random distribution in space (area skill score = 0.5).

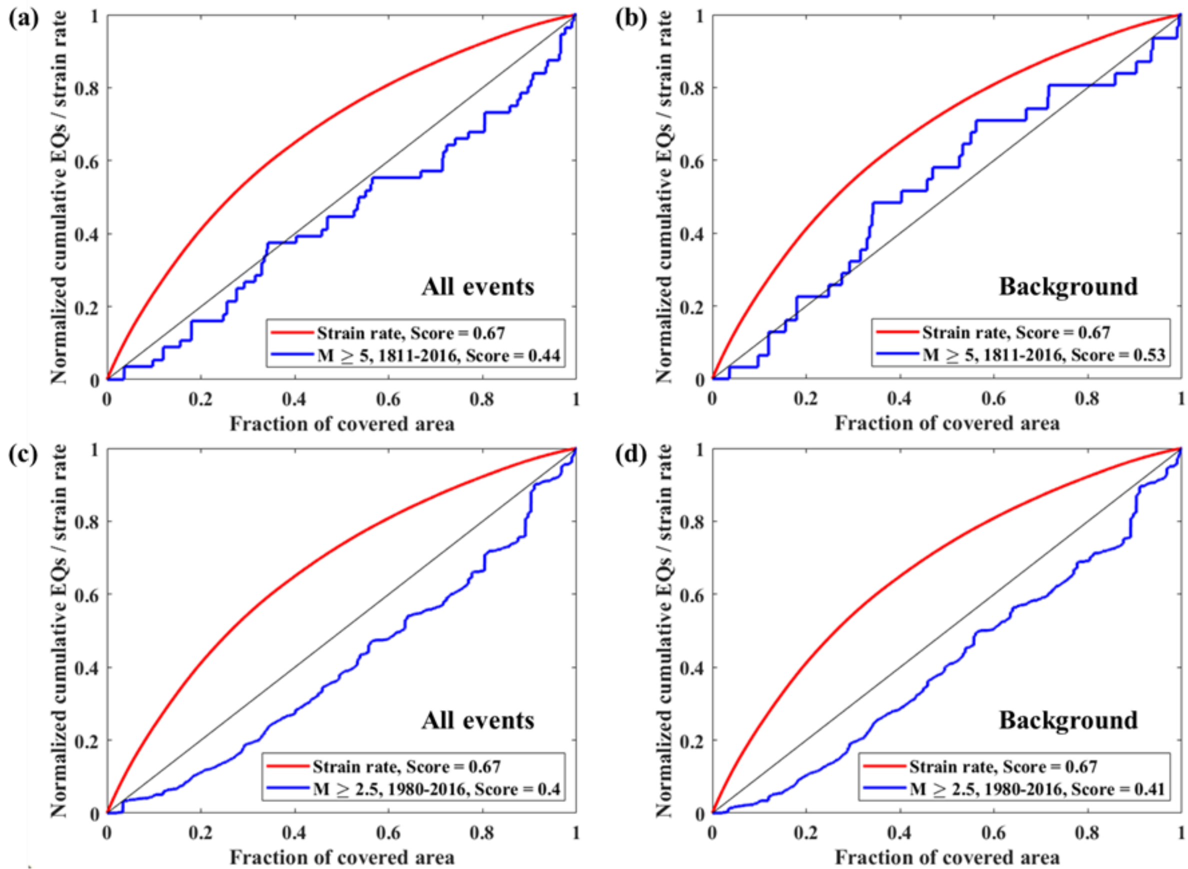

Figure 5. Comparison of the correlations between strain rate and seismicity in the CEUS for **(a)** all events, **(b)** background events of $M \geq 5$ between 1811 and 2016. **(c-d)** Same as (a-b) but for $M \geq 2.5$ events between 1980 and 2016. The background seismicity is obtained by declustering the catalog using the nearest-neighbor method.

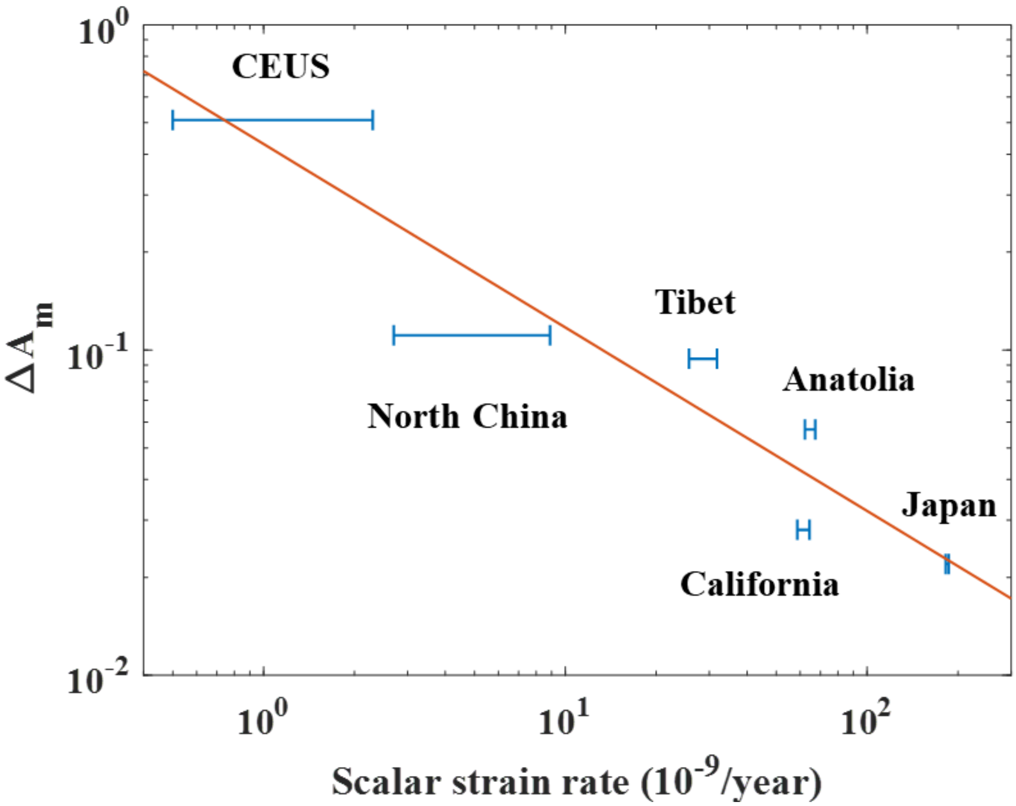

Figure 6. Relationship between mean strain rate and ΔA_m (the fractional area between the strain rate curve and seismic moment curve) based on the results in Table 1. Regions with higher strain rate have smaller values of ΔA_m, which indicates better correlation between strain rate and seismic moment release in higher strain rate regions. The red line is the least-square fitting.

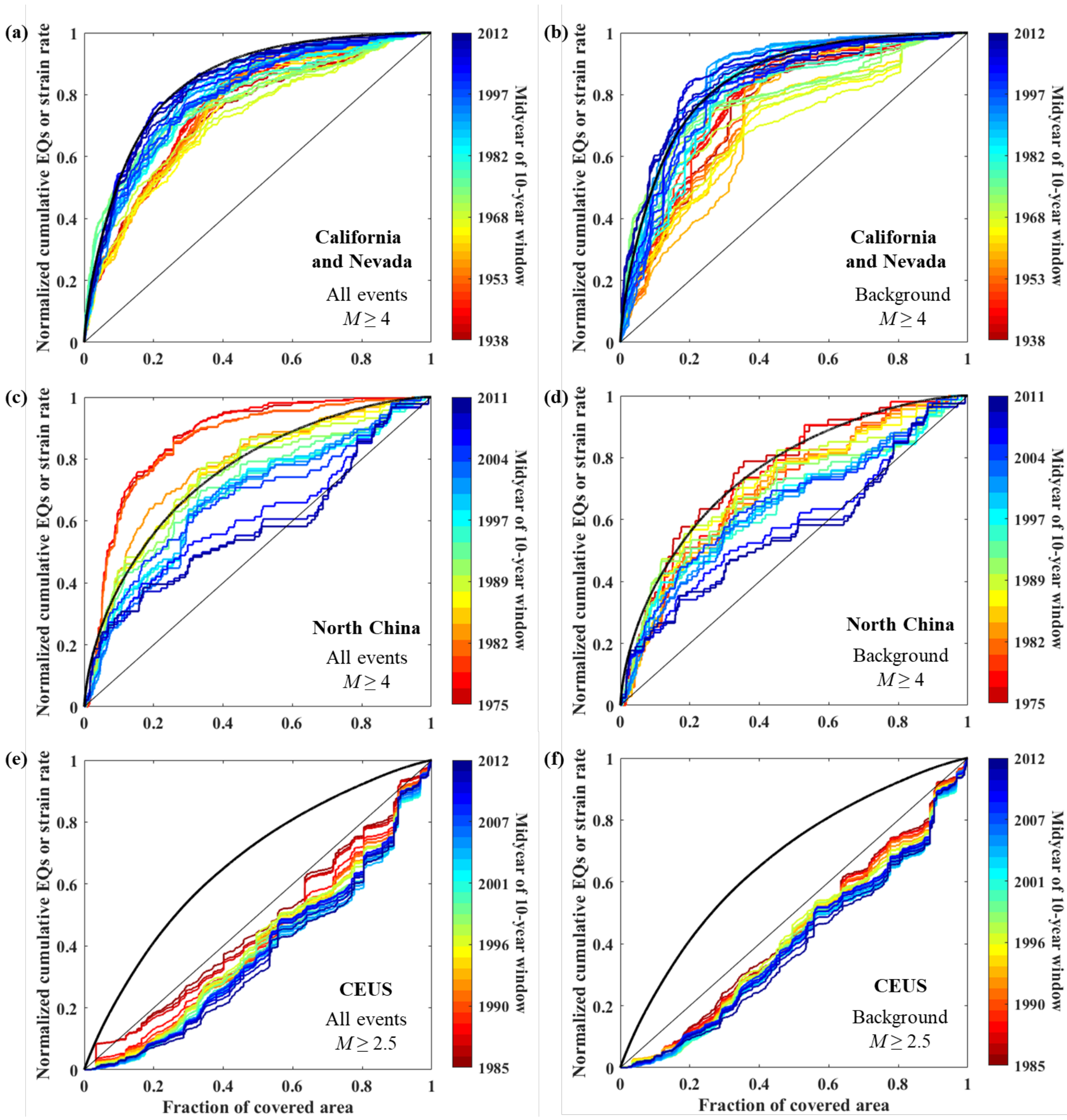

Figure 7. Temporal variations of strain rate-seismicity correlation in California and Nevada for **(a)** all $M \geq 4$ events or **(b)** $M \geq 4$ background earthquakes. The cumulative earthquakes are counted within a 10-year window that moves in 2-year steps from 1933 to 2016. **(c-d)** Same as (a-b), but for $M \geq 4$ earthquakes in North China from 1970 to 2015. **(e-f)** Same as (a-b), but for $M \geq 2.5$ earthquakes in the CEUS from 1980 to 2016. The color bar shows the midyear of the

moving 10-year windows used to calculate the cumulative earthquake counts. The thick black curve is the cumulative strain rate. The diagonal line indicates a spatially random distribution.

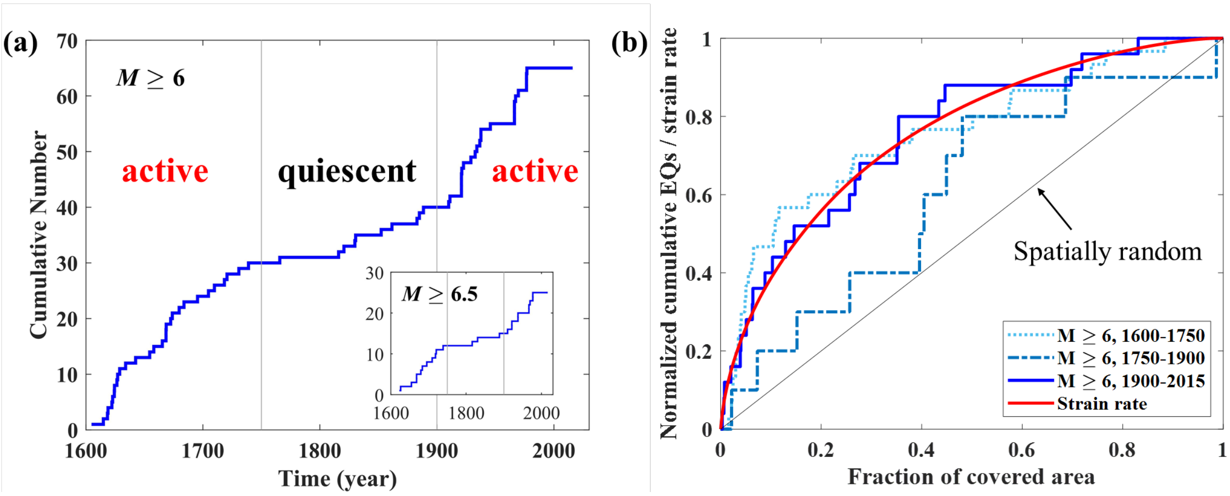

Figure 8. (a) Temporal pattern of $M \geq 6$ earthquakes ($M \geq 6.5$ for inset) in North China with two active periods (1600-1750 and 1900-2015) separated by a relatively quiescent period (1750-1900). **(b)** Comparison of correlations between strain rate (red curve) and seismicity in these three periods. The diagonal line indicates a random distribution of earthquakes.